nature portfolio

https://doi.org/10.1038/s41586-026-10939-0

Supplementary information

Somatic mutations reveal the ontogeny of microglia in human ageing

In the format provided by the authors and unedited

Supplementary Information for

Somatic mutations reveal the ontogeny of microglia in human aging

J.A. Belk *et al.*

Address correspondence to: Julia A. Belk (jbelk@stanford.edu), Howard Y. Chang (howchang@stanford.edu), and Siddhartha Jaiswal (sjaiswal@stanford.edu)

Table of Contents

Supplementary Notes 1-4

- **Supplementary Note 1**
  Design guidelines for hybridization capture PACT panels.
- **Supplementary Note 2**
  Clinical history and neuropathological findings from RA1 and RA2.
- **Supplementary Note 3**
  Additional discussion of human genetic associations of CH and AD.
- **Supplementary Note 4**
  Additional discussion of human microglia replacement.

Supplementary Figures 1-9

- **Supplementary Figure 1**: Variant calling and sort scheme for PACT.
- **Supplementary Figure 2**: Retrospective analysis of informative variants for PACT.
- **Supplementary Figure 3**: Quality control and marker genes for snATAC-seq data.
- **Supplementary Figure 4**: Cell type composition and additional data for snATAC-seq samples.
- **Supplementary Figure 5**: Additional mtscATAC-seq data from BMT recipient RA1.
- **Supplementary Figure 6**: Additional mtscATAC-seq data from RA2.
- **Supplementary Figure 7**: Analysis of brain perivascular macrophages in RA1 and RA2.
- **Supplementary Figure 8**: Infiltrating myeloid cells in the brain of RA1 and RA2 are similar to microglia at additional gene loci.
- **Supplementary Figure 9**: Associations of CH and AD dementia in additional ADSP cohorts.

Legends for Supplementary Tables 1-23

References for Supplementary Information

Supplementary Note 1. Design guidelines for hybridization capture PACT panels.

There are several considerations for the design of custom panels for mutation profiling. This note expands upon the analyses shown in **Supplementary Figures 1 and 2**. Generally, we designed the custom panels in this manuscript to maximize the number of detected variants per person. Overall, in ACT2-7, 49.6% of all variants included in the panel were detected within the brain, either as myeloid-enriched or non-specific variants (**Supplementary Figure 2a-b**). 81.65% of detected mutations were called by both Mutect2 v4.1 and v4.6 and 60.56% of detected mutations were transitions (**Supplementary Figure 2a-d**). Based on these results, it is possible to reduce the number of variants per person to increase the number of individuals that can be profiled with a fixed panel size, if desired. Below, we outline design considerations for PACT panels.

1. **Clone size of interest.** To capture large clones, it is necessary to include higher allele-frequency (AF) variants. However, there are many germline (nonspecific) variants with allele frequencies in the range of 0.35 – 0.65. Thus, there is a tradeoff between including more variants and ensuring that the number of variants is feasible to synthesize. We found that an AF cutoff of 0.40 balanced these two constraints well, typically leading to <1000 variants per person, and was still able to track large clones with cell fractions exceeding 80%, such as in the case of ACT3 (**Supplementary Figure 1**). For more typical clone sizes of 10-30% cell fraction, lower AF cutoffs could be used, reducing the number of variants needed.

2. **Variant calling software.** For our initial experiments, we included variant calls from both Mutect2 v4.1 and v4.6 (**Supplementary Figure 2c**). We found that both versions called most detected variants. We used Mutect2 v4.6 for most experiments, because Mutect2 v4.6 recovered 92.30% of all detected variants. However, we found that the consensus variant calls were enriched in detected variants. Thus, an alternate strategy which we did not pursue here would be to use the consensus calls only, which may reduce the number of undetected variants and make it more feasible to profile more individuals with a fixed number of variants.

3. **Transitions versus transversions.** We observed that 60.56% of detected variants were transitions and 82.23% of undetected (possibly artefactual) variants were transversions (**Supplementary Figure 2d**). Nonetheless, we also included transversions in the panel designs in order to maximize the total number of detected variants per person. For ACT2 – ACT7, there were an average of 217.83 detected mutations when considering transitions only, and 357.50 when both transitions and transversions were included. An alternate strategy would be to include transitions only to reduce the number of variants per person.

4. **Other variants of interest.** It can be useful to include additional variants of interest in each panel. For example, in the present study, we included probes targeting a known list of CH-associated SNV or INDEL exons in each panel. Probes targeting the mitochondrial genome, cancer-associated variants, or other locations of interest could also be straightforwardly included in the panel design.

Supplementary Note 2. Clinical history and neuropathological findings from RA1 and RA2.

Exact ages and certain clinical details of RA1 and RA2 have been redacted to preserve patient privacy.

RA1 – clinical history summary

RA1 was a female who died in her early sixties. RA1 was diagnosed with breast cancer in her late thirties and was treated via mastectomy, radiation, and chemotherapy (Carboplatin, Taxol, Doxorubicin, Cyclophosphamide, and Tamoxifen). 27 months prior to death RA1 was diagnosed with therapy-related myeloid neoplasm and was treated with Decitabine, Venetoclax, and bone marrow transplantation. The transplant occurred 22 months prior to death. She relapsed 11 months later and ultimately died of acute leukemia.

RA1 – postmortem neuropathological findings

The neuropathological evaluation revealed leptomeningeal involvement by therapy-related leukemia. The cystic lesion in the frontoparietal region seen on MRI was identified on gross evaluation and confirmed to be an arachnoid cyst under microscopic examination. Arachnoid cysts are benign structures that can be congenital or acquired. They are rarely symptomatic in adults and are often found incidentally.

Histologic sections of the frontal lobe and to a lesser extent the occipital lobe show a mild lymphocytic leptomeningeal infiltrate which is CD34 and p53 immunopositive, thus signifying a leptomeningeal leukemic infiltrate. A cyst wall composed of a single layer of meningothelial cells consistent with an arachnoid cyst is appreciated. Other sections show no significant abnormality.

RA1 – bone marrow findings leading to myeloid neoplasm diagnosis

Bone marrow aspirate was aspiculate and markedly hemodilute. The biopsy showed a markedly hypocellular core (10%) with marked marrow fibrosis with clustering of CD34+, CD117+ blasts and scattered megakaryocytic dysplasia. A blast count performed on a rare spicule within the marrow yielded 6% blasts (albeit I suspect this is undercounted if proper spicule). There were paratrabecular areas where CD34 clustering was increased with corresponding increased p53 expression. The morphologic and immunophenotypic findings are therefore compatible with a high-grade myeloid neoplasm with marked marrow fibrosis.
DX: MDS-EB1
Karyotype: Complex karyotype 46,XX,del(5)(q13q33)[1]/44,idem,add(6)(p25),-7,del(8)(q22q23),-21,-22,+mar[6]/46,XX[13]
Heme-STAMP (somatic variants): TP53 E286G (Likely Pathogenic, VAF4%) and U2AF1 Q157R (Pathogenic, VAF 3%)
R-IPSS score: 6.5 (very high risk)

RA1 – bone marrow findings at death

Targeted panel sequencing of CH-associated SNV or INDEL exons (**Supplementary Table 4**) revealed the same somatic variants identified at diagnosis via Heme-STAMP analysis (above). U2AF1 Q157R was present at a VAF of 0.182 and TP53 E286G was present at a VAF of 0.186 at death.

RA2 – postmortem neuropathological findings

Sequential coronal sections of the cerebrum display a thrombus in the right M1 territory and an area of infarct involving the right frontal lobe, basal ganglia, insula, and temporal lobe. The remainder of the brain shows a well-defined gray/white matter junction. The cortex is not atrophic. The centrum semiovale is normal. The corpus callosum is of normal thickness. The corpus striatum is unremarkable. The left thalamus and other subcortical nuclei are normal. The ventricular system is symmetrical and not dilated.

Sequential transverse sections of the brain stem perpendicular to its long axis display a normally pigmented substantia nigra and locus ceruleus. The basis pedunculi are symmetrical. The basis pontis is unremarkable. The medulla displays normal inferior olives and symmetrical pyramids. Sagittal sections of the vermis and parasagittal sections of the cerebellum display normal folia and white matter. The dentate nucleus is unremarkable.

Histologic sections stained with H&E confirm recent infarction affecting the right middle cerebral artery territory, as well as confirm the grossly observed thromboembolus in the right middle cerebral artery, M1 segment. Additionally, there are numerous Alzheimer type II astrocytes (metabolic astrocytes) in the right frontal and other grey matter.

RA2 – bone marrow findings at death

Targeted panel sequencing of CH-associated SNV or INDEL exons (**Supplementary Table 4**) did not reveal any putative driver mutations in the bone marrow of RA2.

Supplementary Note 3. Additional discussion of human genetic associations of CH and AD.

Our study adds to the growing body of literature linking the presence of CH clones in the blood to reduced risk of AD[1-3]. In the current work, we expand this concept to show large clones with unknown drivers also show a protective association with AD. This is perhaps not surprising, as genome wide association studies of clonal hematopoiesis with unknown drivers have shown a high degree of genetic correlation to CH with known drivers, especially non-DNMT3A SNV/indel CH[4], indicating many of the unknown driver clones share a similar biology to these known driver clones. Furthermore, since unknown driver clonal hematopoiesis is common and has a protective association with AD, past studies which did not account for this phenomenon likely underestimated the protective association of CH with AD since the control group would have included some people with unknown drivers. Below, we outline recent literature and important considerations for association studies between CH and AD.

1. Causal associations between CH and human disease risk are expected to be stronger for individuals with larger CH clones. This is because larger numbers of mutant cells would be expected to collectively exert larger functional effects, an idea that has been confirmed empirically in several studies. For example, epidemiological associations of clonal hematopoiesis have found that the risk of hematological malignancies[5-7], atherosclerotic cardiovascular disease[8,9], chronic liver disease[10], and chronic obstructive pulmonary disease[11] is greatest in those with larger clone size (typically defined as >0.1 variant allele fraction). This idea is not specific to CH; larger functional impacts of larger somatic clones has also been shown in other neurological disease contexts (discussed in point 4, below)[12]. Consistent with a causal association, multiple papers have now shown that larger CHIP clones in blood show the greatest protective associations for AD[1,3]. A causal role for mutant CH cells in reducing AD incidence has also been demonstrated in humans via Mendelian Randomization analyses[1] and is consistent with functional experiments in mice and iPSCs (discussed in point 3, below)[2,13].

2. Cell type quantification is essential for CH variant interpretation, especially in complex tissues like the human brain. A recent study performed deep sequencing of whole brain DNA samples from deceased individuals with or without AD and found an increased burden of low VAF CH variants in individuals with AD[13]. The effect size was strongest in those with small clones that were below the limit of detection in blood whole exome sequencing[13]. Because low VAF CH variants are ubiquitous in aged individuals[14], these findings suggest that the presence of AD may lead to an enhanced ability to detect low VAF CH variants. For example, AD causes neuronal loss[15,16] which may enhance detection of small CH clones by increasing the proportion of microglia and other immune cells relative to neurons. In addition, analyzing bulk brain tissue (without digesting the tissue to obtain intact nuclei) likely includes sequencing reads from non-parenchymal cells and/or dying immune cells adhered to amyloid plaques, such as granulocytes[17,18]. Future studies comparing CH variant presence and clone size in sorted microglial nuclei in those with and without AD will be needed to fully clarify why the presence of AD seems to lead to the detection of more small CH clones in the brain.

3. Clearance of β-amyloid by microglial phagocytosis can be beneficial in Alzheimer's Disease. Multiple groups have begun studying CH in the context of AD using model systems[2,13]. In mice, transplantation of *Tet2*-KO bone marrow into 5XFAD mice demonstrated that mutant cells have an enhanced ability to invade the brain and clear β-amyloid, translating to reduced cognitive decline[2]. Induced pluripotent stem cells (iPSCs) engineered with CH mutations and differentiated into microglia were more phagocytic and had a more pro-inflammatory transcriptional profile, resembling the disease-associated

microglia (DAM) phenotype[2,13,19]. These findings are consistent with the idea that CH may mitigate AD incidence via enhanced phagocytosis of β-amyloid. In particular, the DAM is highly phagocytic and can have a protective role in AD[19,20]; for example, genetic studies of TREM2 knockout animals, which do not form the DAM, exhibit accelerated β-amyloid accumulation and neuronal loss[19,21]. The importance of phagocytosis in clearing β-amyloid is further supported by human genetics, where multiple rare and common variants in genes including TREM2, PLCG2, and CD33 have been identified that act via this pathway[22]. Although one recent study hypothesizes that the DAM phenotype induced in CH-mutant iPSC cells may exacerbate AD[13], this concept is not supported by functional data at present. Functional assays generated from similar iPSC cultures were previously published, demonstrating that these cells exhibit enhanced phagocytosis of β-amyloid and supporting a model in which CH mitigates AD neuropathology and cognitive decline[2]. Overall, the DAM phenotype and clearance of β-amyloid more generally can be protective in AD[23], and may contribute to the protective association between CH and AD.

4. Non-CH somatic variants have been previously associated with AD. Elegant work from Frederic Geissmann and others has shown that non-CH somatic variation, specifically variants in the mitogen-activated protein kinase pathway (BRAF, CBL, NF1, KRAS, and others), are associated with neurodegeneration and Alzheimer's disease[12,24,25]. Supporting a causal role for these clones, larger clones were associated with neurological symptoms, and causality was also shown using mouse models[12,24]. Thus, somatic variation in microglia must be considered in terms of the driver event and developmental origin (yolk sac versus hematopoietic stem cell) of each clone, with distinct categories of variants likely playing distinct roles in human disease contexts.

Collectively, findings from multiple investigators provide additional support for the idea that large CH clones are associated with protection from AD in autopsy-confirmed cohorts and in longitudinal cohorts, where CH clones are present prior to the onset of AD. Separately, AD may enhance the ability to detect small CH clones in the brain, perhaps due to neuronal death increasing the relative proportion of microglia[13]. Several lines of evidence thus support a causal role for large CH clones in reducing AD dementia and AD neuropathology, potentially via enhanced phagocytosis by the mutant cells[1,2]. These studies support the idea that engineering peripheral myeloid cells to enhance clearance of β-amyloid and tau tangles within the brain may be a therapeutic hypothesis that warrants further investigation in AD.

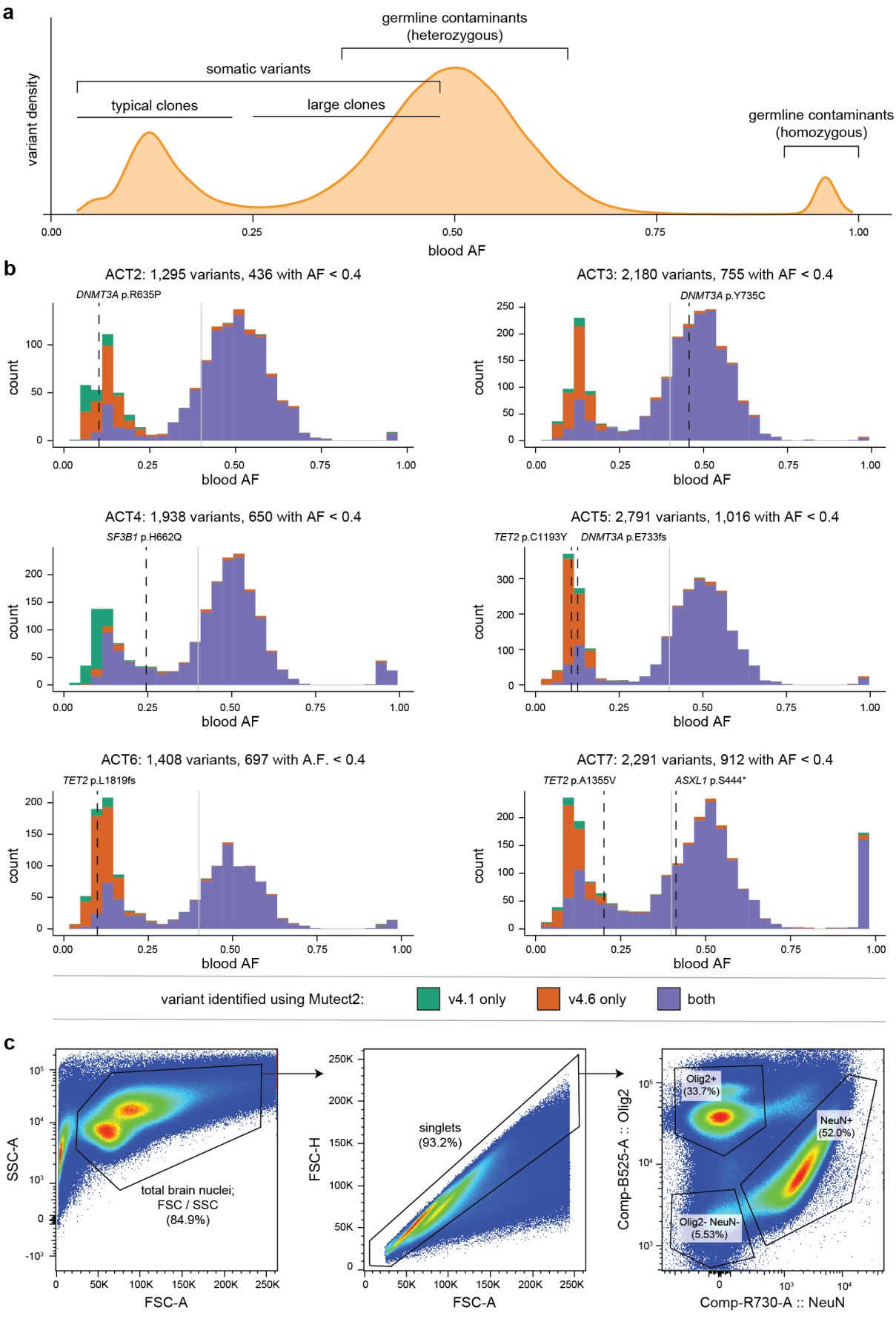
Supplementary Note 4. Additional discussion of human microglia replacement.

Our data support the idea that there is a polyclonal invasion of peripheral immune cells into the brain at some point during human aging. We find that peripheral clones caused by any type of driver mutation, including clones without known driver mutations, can be found in the brain in older individuals at similar cell fraction as seen in the blood. This suggests that specific mutations are not determinative for brain infiltration. Instead, we hypothesize that this influx is caused by the pool of yolk sac microglia contracting (or collapsing) at some point during aging, triggering a partial or complete replacement of the brain myeloid niche from the periphery. These newly engrafted cells may outcompete remaining yolk sac microglia for available niche space, eventually resulting in complete replacement of the microglial pool. Future work will be needed to fully understand microglia replacement in humans, but this model is supported by the following major points from our work and others:

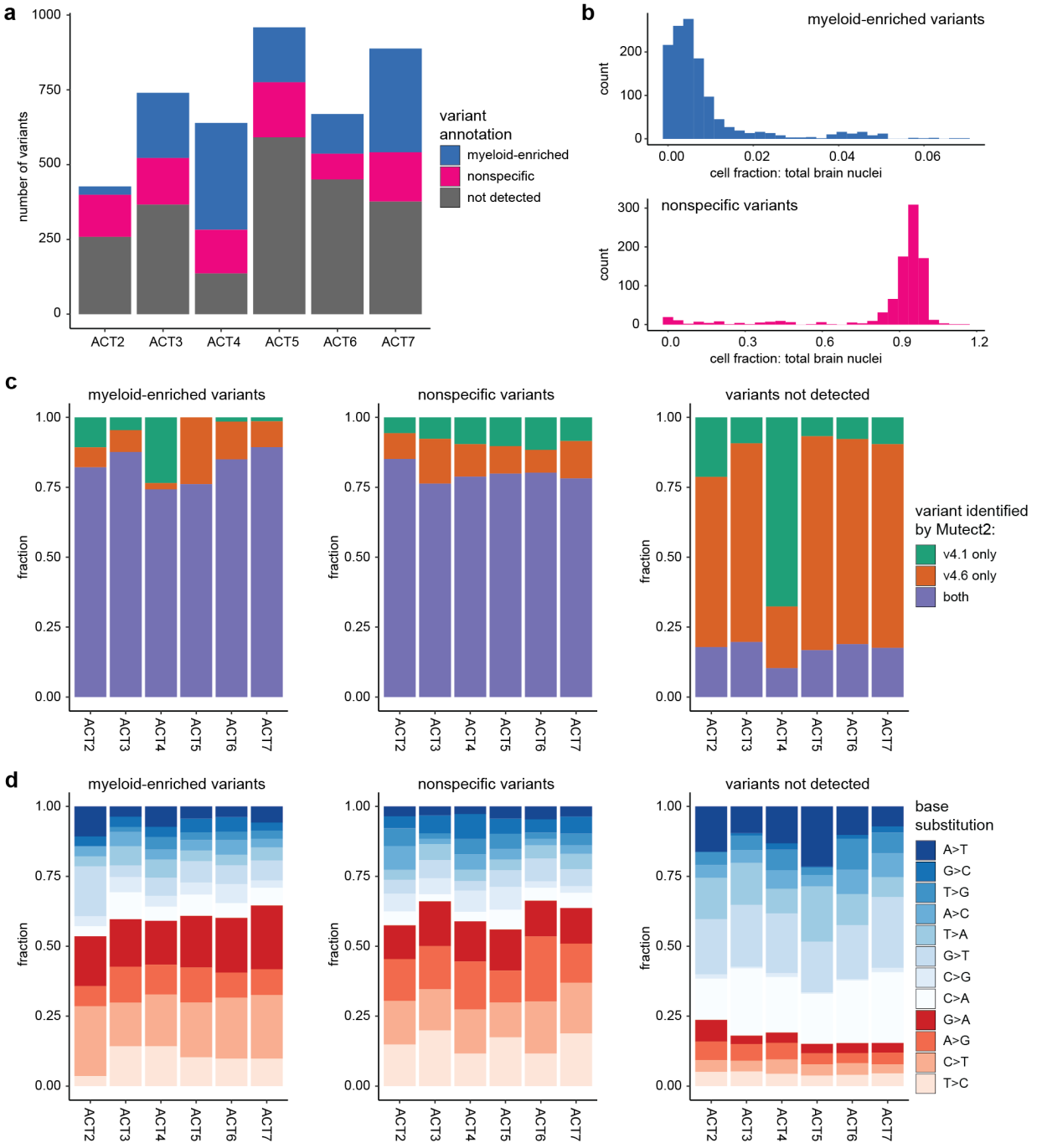
1. **In mice, depletion of endogenous microglia causes microglia replacement**, even in mice that are not perturbed in any other way (i.e., not transplanted or irradiated)[26].
2. **Bone marrow clones appear to equilibrate with the brain niche**. In our data, in the oldest individuals (80+ years old), there is a strong correlation between the clone size in the periphery and in the brain (Figure 2f). This may be because the brain myeloid niche is empty (i.e., the yolk sac microglia are gone) and the bone marrow and brain niches are equilibrating.
3. **Mutant and wild type microglia are almost identical**. The data shown in Extended Data 7e-f and in Figure 3 demonstrate that mutant microglia (microglia harboring LoY or m.2098C) are similar to the unlabeled microglia in the brain. The similarity between both microglia genotypes may be explained by a total replacement of microglia from the periphery. Specifically, the “wild type” cells in these analyses may also be of bone marrow origin.
4. **All clones are able to colonize the brain**. Our data show that many clones, regardless of driver mutation, invade the brain with aging. These data support a “niche-intrinsic” model, where contraction or absence of yolk sac microglia equally recruits all types of bone marrow myeloid cells into the brain, rather than a “clone-intrinsic” model where specific driver mutations are necessary for brain infiltration. The deeper analysis of mtDNA variants that is included in Extended Data Figure 12 further supports this idea, revealing a polyclonal invasion of peripheral immune cells into the brain of RA2. Larger studies of specific driver mutations will be needed to test whether there are more subtle differences in capacity to engraft the brain across different drivers.

A major caveat is that PACT relies on age-associated somatic mutations and clonal expansions to detect microglia replacement. It is possible that the peripheral infiltration begins earlier than 73 years of age.

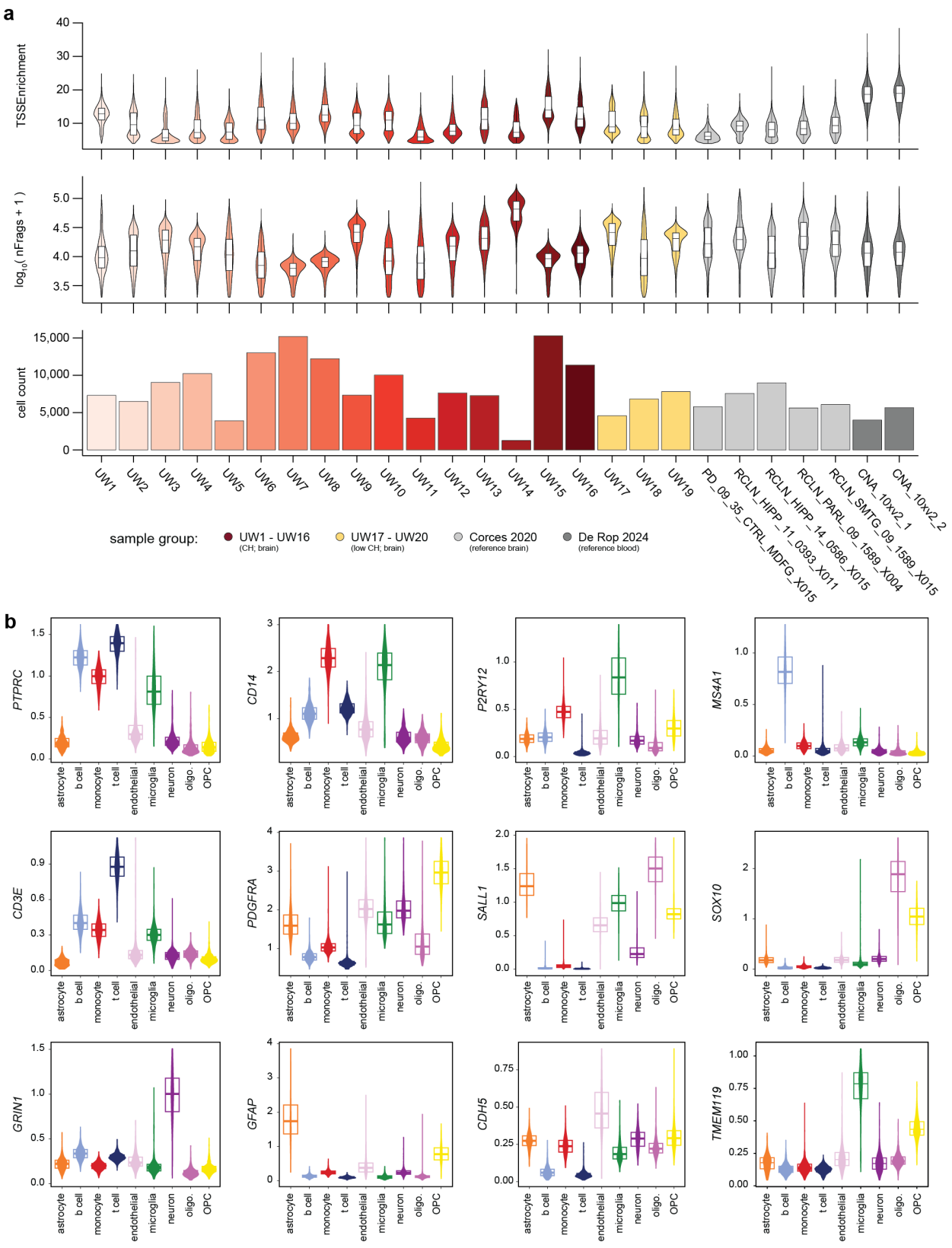
Supplementary Figures 1-9



Supplementary Figure 1: Variant calling and sort scheme for PACT. (a) Schematic of typical variant calling results in human blood by allele frequency (AF). **(b)** Variant calling results for each ACT subject by AF. Cutoff for inclusion in the PACT panel (AF < 0.4) is shown in gray. Known SNV/INDEL driver(s) are shown as dashed lines. **(c)** Representative sort scheme for sorting human brain nuclei for PACT.

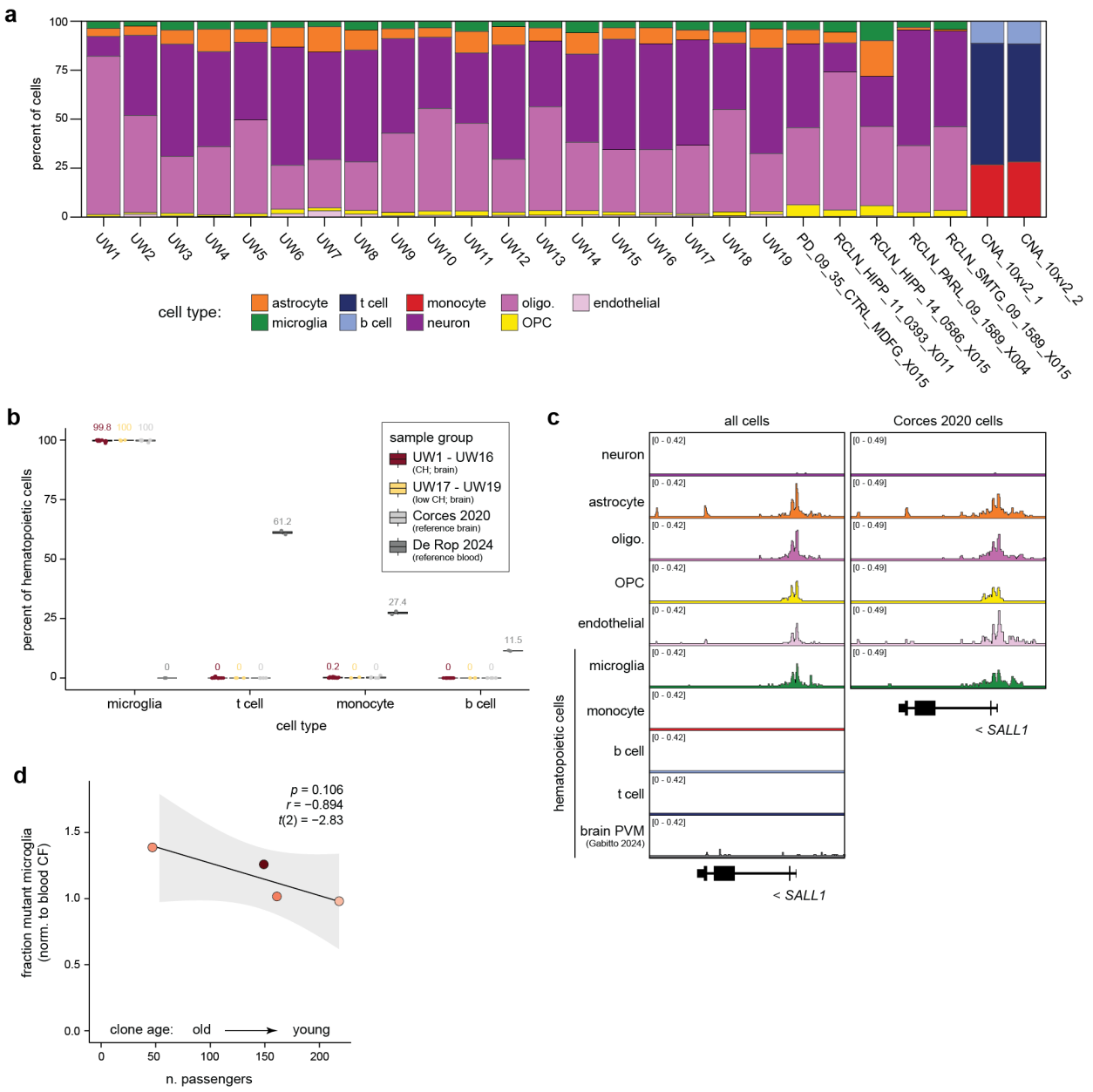


Supplementary Figure 2: Retrospective analysis of informative variants for PACT. (a) Number of mutations identified as myeloid-enriched, nonspecific, or not detected from PACT results of each individual. **(b)** Histogram of the brain cell fractions of PACT variants for myeloid-enriched variants (top) and nonspecific variants (bottom). **(c)** Analysis of Mutect2 performance for each variant category and each individual. **(d)** Analysis of base substitutions (transitions or transversions) for each variant category and each individual.

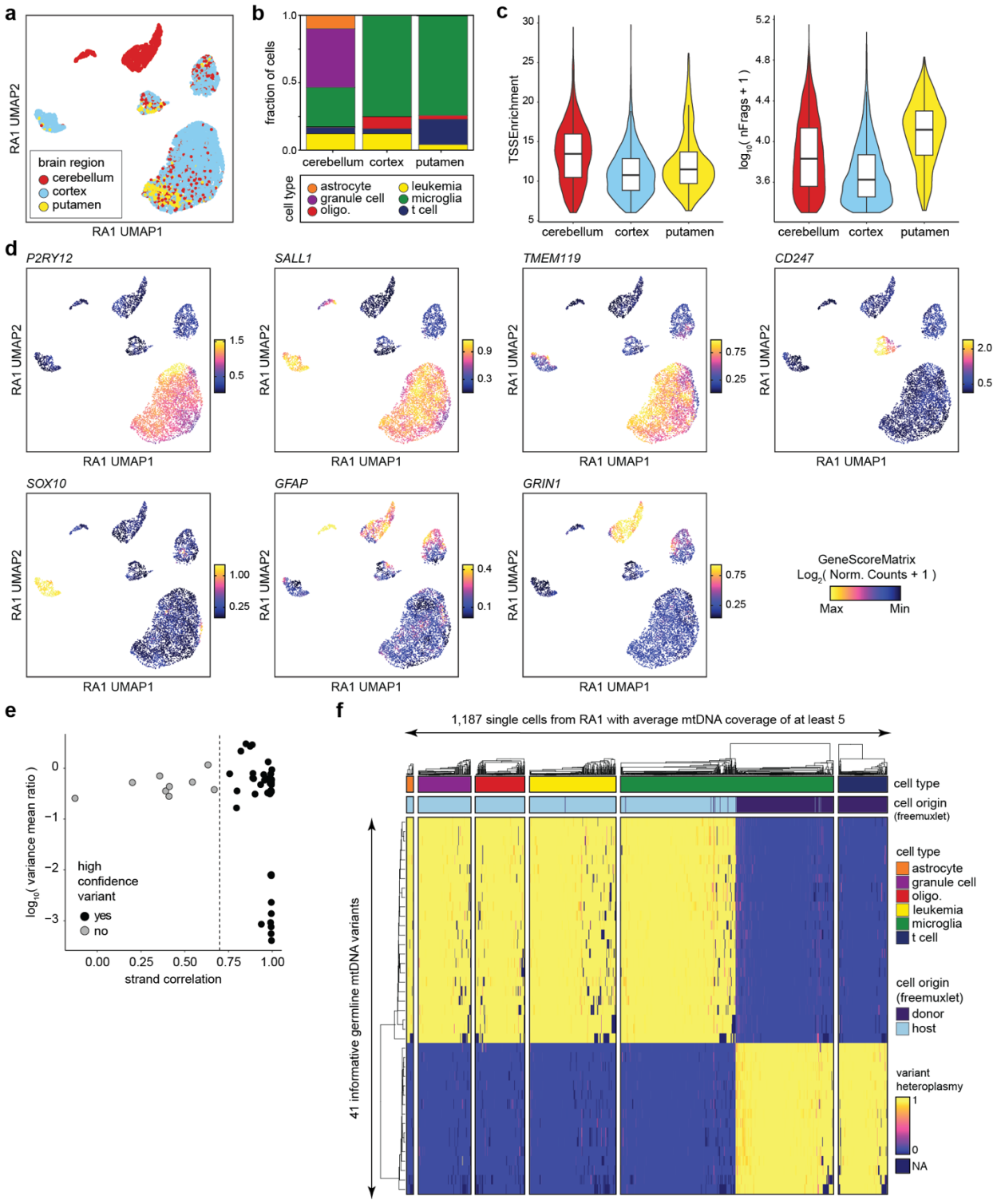


Supplementary Figure 3: Quality control and marker genes for snATAC-seq data. (a) snATAC-seq metrics for each sample in the present study, as well as each sample included from brain and blood reference datasets. TSS enrichment per cell (top), number of fragments per cell (center), and number of cells (bottom) are shown for each sample. **(b)** Quantification of gene

accessibility for selected marker genes in each snATAC-seq cell type. Gene accessibility is quantified using ArchR GeneScore. **(a-b)** A median of n=7,326 nuclei were analyzed per snATAC-seq sample; n for each sample and cell type is provided in Supplementary Table 6. Box plots show the median, first quartile and third quartile. Box plot whiskers show minimum and maximum values, which are capped at a distance of 1.5 × (interquartile range) away from the box.

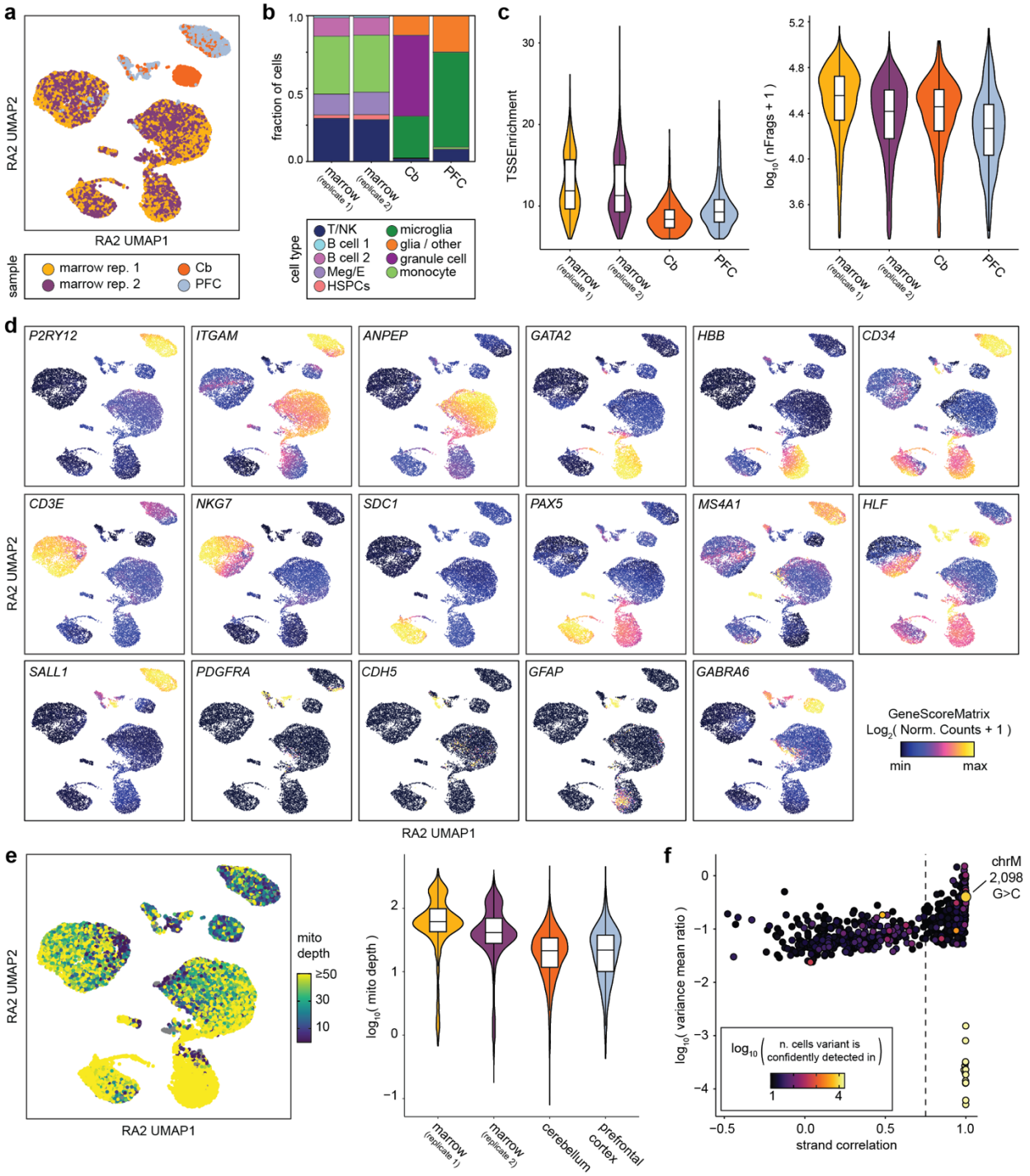


Supplementary Figure 4: Cell type composition and additional data for snATAC-seq samples. (a) Proportion of nuclei assigned to each snATAC-seq cell type for each sample included in Figure 2. **(b)** Quantification of immune cell composition of each sample in Figure 2. Median percentage in each group is indicated above each boxplot. N=26 samples were analyzed; n=16 CH brain samples, n=3 low CH brain samples, n=5 reference brain samples, and n=2 reference blood samples. Box plots show the median, first quartile and third quartile. Box plot whiskers show minimum and maximum values, which are capped at a distance of 1.5 × (interquartile range) away from the box. **(c)** Pseudobulk snATAC-seq tracks for indicated cell types at the *SALL1* locus for all cells in Figure 2 (left) and cells from Corces 2020 only (right). **(d)** Correlation between the fraction mutant microglia, normalized to blood clone size, and the number of passenger mutations present on the clone. n=4 samples with equal or more mutant microglia than mutant blood cells. Statistical significance was assessed by two-sided Pearson's product-moment correlation using a t-statistic with n-2 degrees of freedom. *r*, *t*, and *p* are indicated numerically and the CI95 is shown in gray.

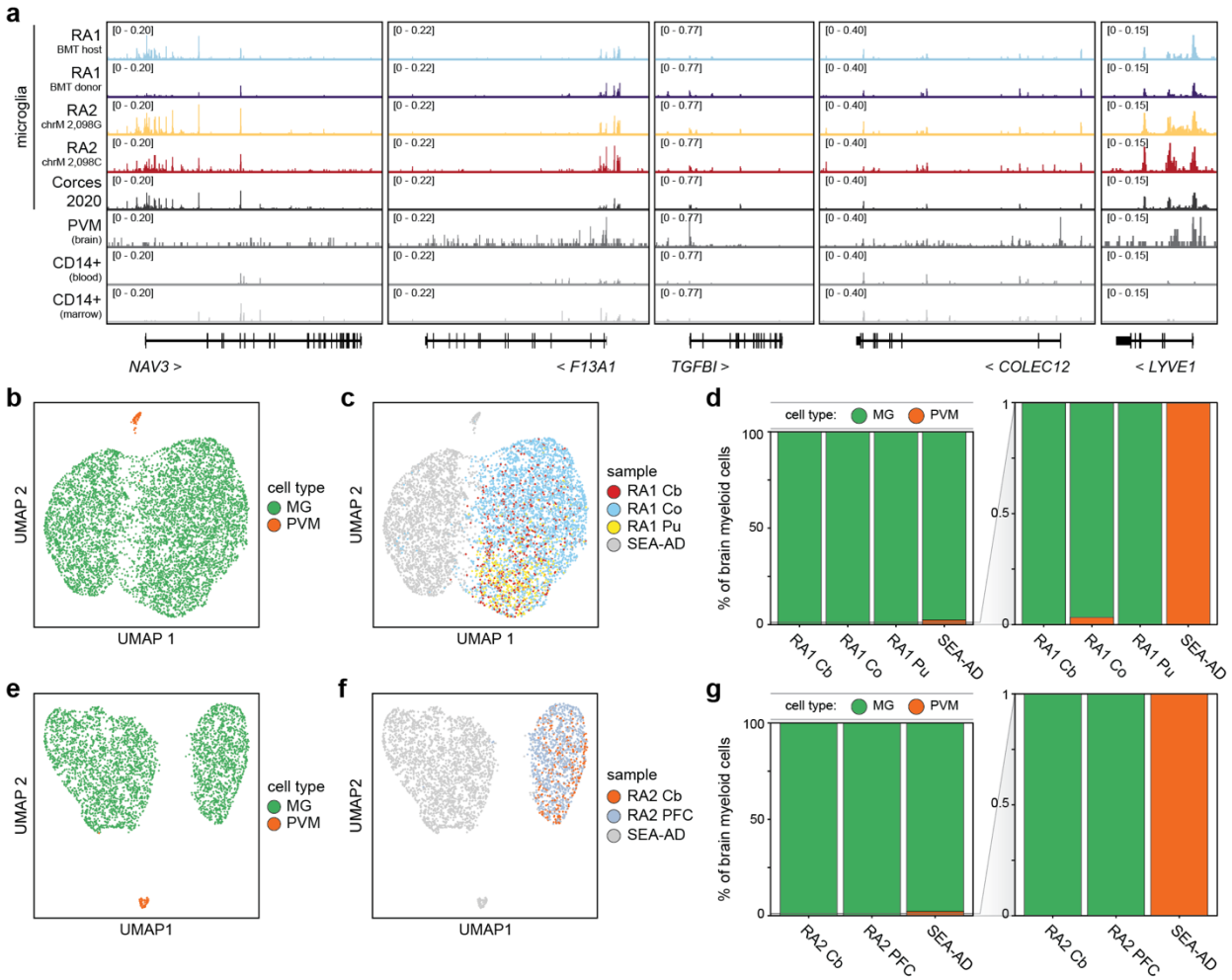


Supplementary Figure 5: Additional mtscATAC-seq data from BMT recipient RA1. (a) scATAC-seq profiles of cells from RA1 colored by brain region. **(b)** Proportion of cells assigned to each cell type for each sample from RA1. **(c)** TSS enrichment per cell (left) and number of fragments per cell (right) for each brain region profiled from RA1. N=6,239 single cells from RA1 profiled with mtscATAC-seq; n=1,591 (cerebellum), n=4,061 (cortex) or n=587 (putamen). Box plots show the median, first quartile and third quartile. Box plot whiskers show minimum and maximum values, which are capped at a distance of 1.5 × (interquartile range) away from the box.

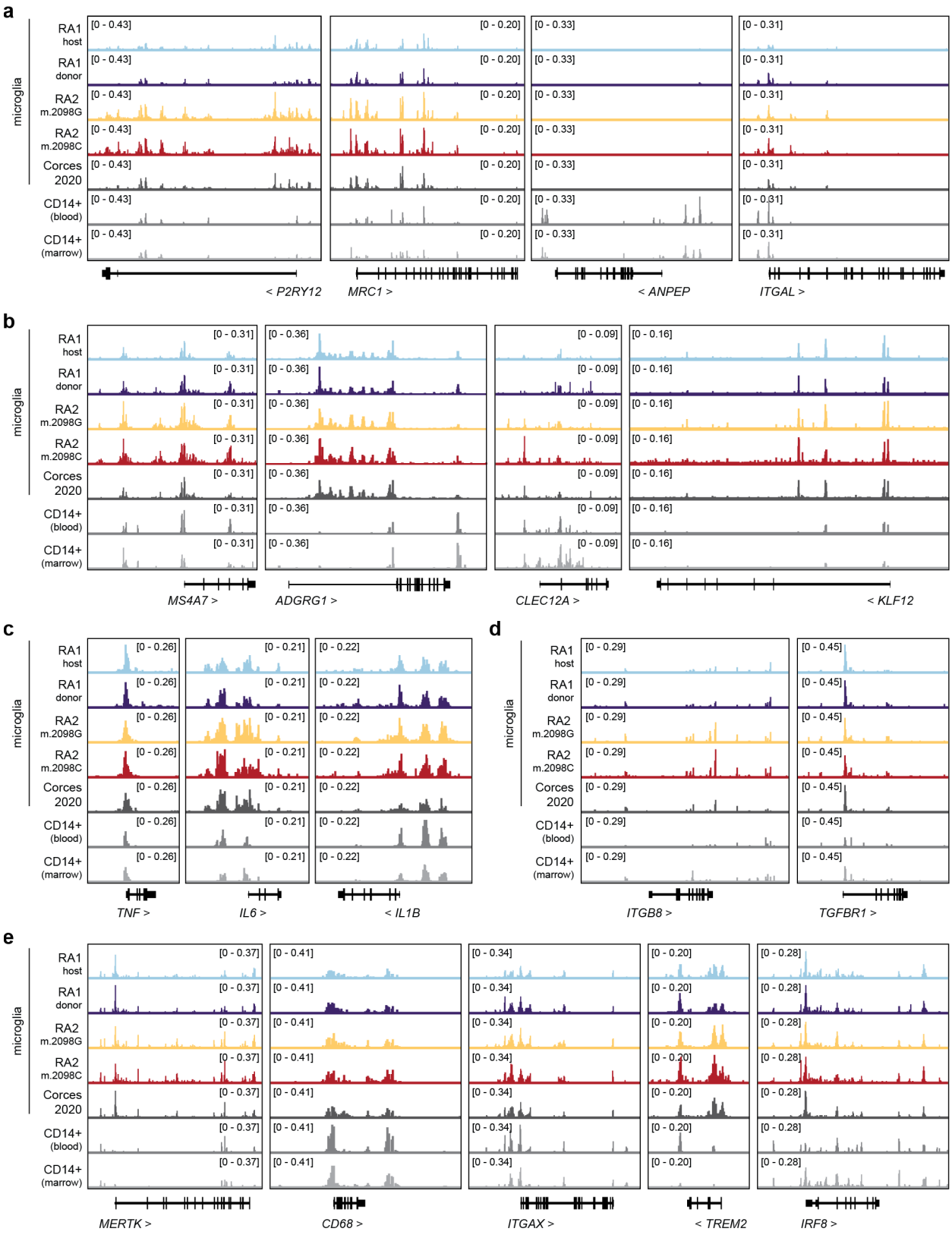
(d) scATAC-seq profiles of cells from RA1 colored by gene accessibility for selected marker genes. **(e)** mtDNA variants identified by mgatk from aggregated RA1 data. **(f)** Concordance of mtDNA genotypes and germline genotypes in single cells from RA1 data. mtDNA genotypes were determined by mgatk; germline genotypes were determined by freemuxlet. Droplets identified as doublets by either genotyping approach were excluded.



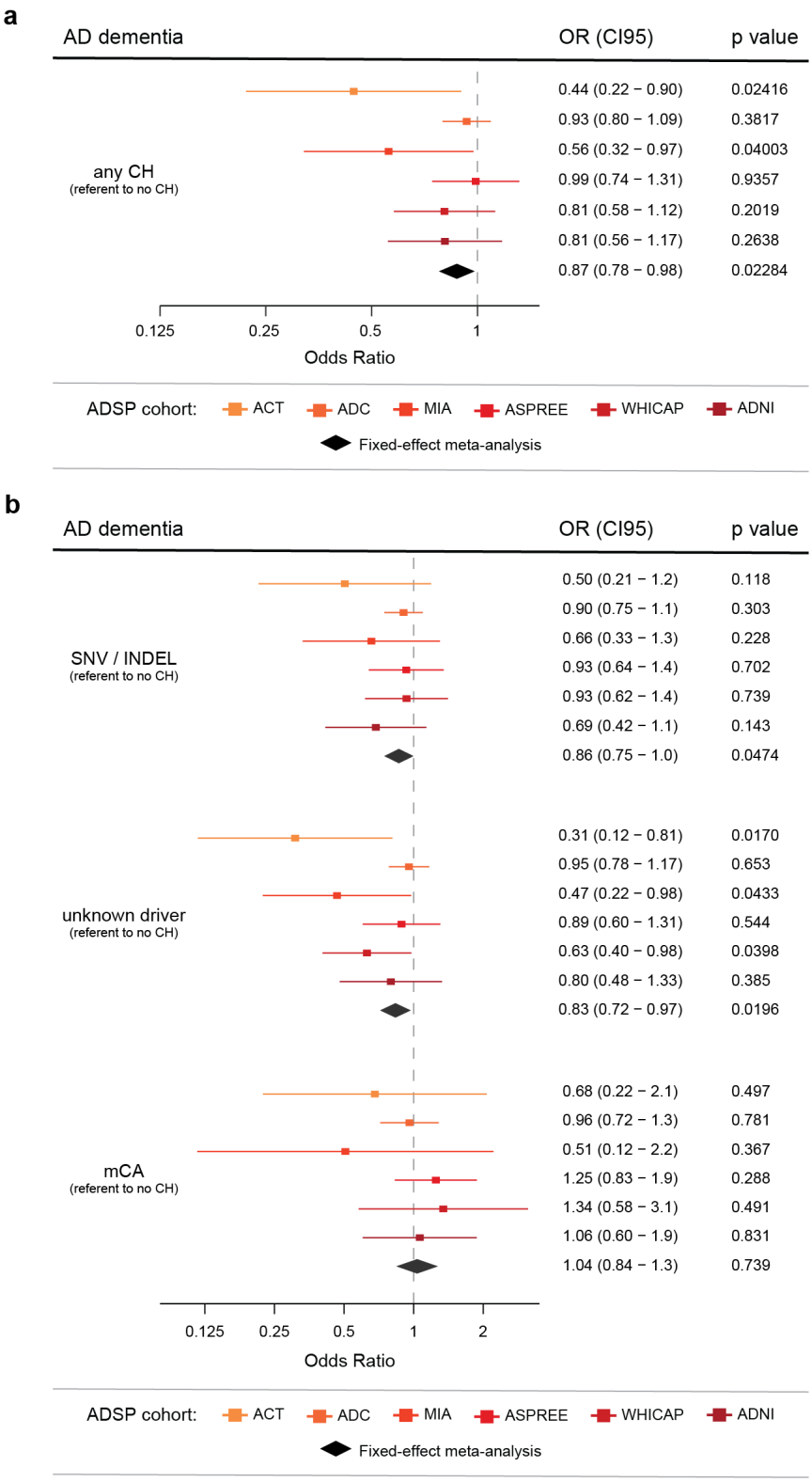
Supplementary Figure 6: Additional mtscATAC-seq data from RA2. (a) scATAC-seq profiles of cells from RA2 colored by sample. **(b)** Proportion of cells assigned to each snATAC-seq cell type for each sample from RA2. **(c)** TSS enrichment per cell (left) and number of fragments per cell (right) for each sample profiled from RA2. **(d)** scATAC-seq profiles of cells from RA2 colored by gene accessibility for selected marker genes. **(e)** Mitochondrial genome coverage as quantified by mgatk in single cells (left) or aggregated by sample (right). **(f)** mtDNA variants identified by mgatk from aggregated RA2 data. Cb, cerebellum; PFC, prefrontal cortex. **(c, e)** N=14,227 single cells from RA2 profiled with mtscATAC-seq; n=5,298 (marrow 1), n=6,388 (marrow 2), n=952 (Cb), or n=1,589 (PFC). Box plots show the median, first quartile and third quartile. Box plot whiskers show minimum and maximum values, which are capped at a distance of 1.5 × (interquartile range) away from the box.



Supplementary Figure 7: Analysis of brain perivascular macrophages in RA1 and RA2. (a) Visualization of selected gene loci for RA1 and RA2 microglia of both genotypes. Reference microglia and brain perivascular macrophages are also included. **(b-c)** Co-clustering of RA1 brain myeloid cells with the SEA-AD microglia and SEA-AD brain perivascular macrophages colored by cluster assignment **(b)** or sample **(c)**. **(d)** Quantification of brain perivascular macrophages in each brain region of RA1. **(e-f)** Co-clustering of RA2 brain myeloid cells with the SEA-AD microglia and SEA-AD brain perivascular macrophages colored by cluster assignment **(e)** or sample **(f)**. **(g)** Quantification of brain perivascular macrophages in each brain region of RA2.



Supplementary Figure 8: Infiltrating myeloid cells in the brain of RA1 and RA2 are similar to microglia at additional gene loci. Pseudobulk scATAC-seq tracks for **(a)** myeloid marker genes[1,27-29], **(b)** brain-infiltrating myeloid cell marker genes[30,31], **(c)** cytokines[8,32,33], **(d)** TGFβ-related genes[29], and **(e)** phagocytosis and disease-associated microglia genes[19,34].



Supplementary Figure 9: Associations of CH and AD dementia in additional ADSP cohorts. **(a)** Effect of CH on the risk of AD dementia. **(b)** Effect of CH driver type on the risk of AD dementia. **(a-b)** include individuals in the ACT (n=172), ADC (n=3,070), MIA (n=353), ASPREE (n=3,066), WHICAP (n=701), and ADNI (n=990) cohorts. Additional demographic information is available in Supplementary Table 23. For longitudinal cohorts (ASPREE, WHICAP, and ADNI) only incident

AD cases were considered. For other cohorts, analysis was restricted to individuals older than 75 at blood draw and older than 65 at time of AD diagnosis. OR, CI95, and two-sided Wald P value were calculated from logistic regression models which included age, sex, and *APOE* genotype as covariates. The measure of center is the OR and the lengths of the lines represent the CI95 for the OR. For meta-analyses, the center of the diamonds represents the OR and the lengths represent the CI95 for the OR.

Legends for Supplementary Tables 1-23

Supplementary Table 1. List of hematopoietic genes and variants queried.
Supplementary Table 2. PACT results for all sorted nuclei fractions of ACT2-7.
Supplementary Table 3. Donor characteristics and PACT results for ACT2-7 and UW1-23.
Supplementary Table 4. Table of genome coordinates included in targeted CH sequencing panel.
Supplementary Table 5. SNV or INDEL variant identification from myeloid-enriched brain samples.
Supplementary Table 6. Cell counts for each cell type and sample (see also Figure 2).
Supplementary Table 7. Calculation of percentage of mutant microglia in each sample (see also Figure 2).
Supplementary Table 8. Cell counts for each cell type and sample - multi brain region clustering (see also EDF 5).
Supplementary Table 9. Calculation of percentage of mutant microglia in each sample - multi brain region (see also EDF 5).
Supplementary Table 10. Differentially accessible genes for perivascular macrophages versus microglia in the SEA-AD multi-ome cohort.
Supplementary Table 11. Differentially active transcription factors (TFs) for perivascular macrophages versus microglia in the SEA-AD multi-ome cohort.
Supplementary Table 12. Differentially accessible peaks for perivascular macrophages versus microglia in the SEA-AD multi-ome cohort.
Supplementary Table 13. Cell counts for each cell type and sample - aging (see also EDF 11).
Supplementary Table 14. Calculation of percentage of mutant microglia in each sample - aging (see also EDF 11).
Supplementary Table 15. Differentially accessible genes for BMT donor versus host microglia in RA1.
Supplementary Table 16. Differentially active transcription factors (TFs) for BMT donor versus host microglia in RA1.
Supplementary Table 17. Differentially accessible peaks for BMT donor versus host microglia in RA1.
Supplementary Table 18. Differentially accessible genes for m.2098C versus m.2098G microglia in RA2.
Supplementary Table 19. Identifying CH without known drivers.
Supplementary Table 20. Prevalence of each type of somatic driver event during human aging.
Supplementary Table 21. Cohort Demographics - AD dementia with ADNC.
Supplementary Table 22. Prevalence of CH drivers - AD dementia with ADNC.
Supplementary Table 23. Cohort Demographics - AD dementia.

References for Supplementary Information

1 Bouzid, H. *et al.* Clonal hematopoiesis is associated with protection from Alzheimer's disease. *Nature Medicine 2023 29:7* **29** (2023-06-15).

2 Matatall, K. A. *et al.* TET2-mutant myeloid cells mitigate Alzheimer's disease progression via CNS infiltration and enhanced phagocytosis in mice. *Cell Stem Cell* **0** (2025).

3 Jakubek, Y. A. *et al.* Clonal hematopoiesis of indeterminate potential and the risk of cognitive impairment in the Women's Health Initiative Memory Study. *Alzheimer's & Dementia* **21** (2025/10/01).

4 Wen, S. *et al.* Clonal haematopoiesis without identified genetic drivers: insights from analyses of 407,512 individuals. *medRxiv* (2026-05-21).

5 Jaiswal, S. *et al.* Age-Related Clonal Hematopoiesis Associated with Adverse Outcomes. *New England Journal of Medicine* **371** (2014-12-25).

6 Abelson, S. *et al.* Prediction of acute myeloid leukaemia risk in healthy individuals. *Nature 2018 559:7714* **559** (2018-07-09).

7 Weeks, L. D. *et al.* Prediction of Risk for Myeloid Malignancy in Clonal Hematopoiesis. *NEJM Evidence* (2023-04-25).

8 Jaiswal, S. *et al.* Clonal Hematopoiesis and Risk of Atherosclerotic Cardiovascular Disease. *New England Journal of Medicine* **377** (2017-07-13).

9 Esra D. Gumuser, M. *et al.* Clonal Hematopoiesis of Indeterminate Potential Predicts Adverse Outcomes in Patients With Atherosclerotic Cardiovascular Disease. *Journal of the American College of Cardiology* **81** (2023-5-23).

10 Wong, W. J. *et al.* Clonal haematopoiesis and risk of chronic liver disease. *Nature 2023 616:7958* **616** (2023-04-12).

11 Miller, P. G. *et al.* Association of clonal hematopoiesis with chronic obstructive pulmonary disease. *Blood* **139** (2022/01/20).

12 Vicario, R. *et al.* Role of clonal inflammatory microglia in histiocytosis-associated neurodegeneration. *Neuron* **113** (2025/04/02).

13 Huang, A. Y. *et al.* Somatic cancer variants enriched in Alzheimer's disease microglia-like cells drive inflammatory and proliferative states. *Cell* **0** (2026).

14 Young, A. L. *et al.* Clonal haematopoiesis harbouring AML-associated mutations is ubiquitous in healthy adults. *Nature Communications 2016 7:1* **7** (2016-08-22).

15 Gómez-Isla, T. *et al.* Profound Loss of Layer II Entorhinal Cortex Neurons Occurs in Very Mild Alzheimer's Disease. *Journal of Neuroscience* **16** (1996-07-15).

16 Terry, R. D. *et al.* Physical basis of cognitive alterations in alzheimer's disease: Synapse loss is the major correlate of cognitive impairment. *Annals of Neurology* **30** (1991/10/01).

17 Migration of neutrophils targeting amyloid plaques in Alzheimer's disease mouse model. *Neurobiology of Aging* **35** (2014/06/01).

18 Smyth, L. C. D. *et al.* Neutrophil-vascular interactions drive myeloperoxidase accumulation in the brain in Alzheimer's disease. *Acta Neuropathologica Communications 2022 10:1* **10** (2022-03-24).

19 Keren-Shaul, H. *et al.* A Unique Microglia Type Associated with Restricting Development of Alzheimer's Disease. *Cell* **169** (2017/06/15).

20 Disease-Associated Microglia: A Universal Immune Sensor of Neurodegeneration. *Cell* **173** (2018/05/17).

21 Wang, Y. *et al.* TREM2 Lipid Sensing Sustains the Microglial Response in an Alzheimer's Disease Model. *Cell* **160** (2015/03/12).

22 Brown, G. C. *et al.* Microglial phagocytosis in Alzheimer disease. *Nature Reviews Neurology 2025 22:1* **22** (2025-11-28).

23 van Olst, L. *et al.* Microglial mechanisms drive amyloid-β clearance in immunized patients with Alzheimer's disease. *Nature Medicine 2025 31:5* **31** (2025-03-06).

24 Mass, E. *et al.* A somatic mutation in erythro-myeloid progenitors causes neurodegenerative disease. *Nature 2017 549:7672* **549** (2017-08-30).

25 Vicario, R. *et al.* A microglia clonal inflammatory disorder in Alzheimer's Disease. *eLife* **13** (2024/9/24).
26 S, D. *et al.* Brain-engrafted monocyte-derived macrophages from blood and skull-bone marrow exhibit distinct properties - PubMed. *Neuron* (03/11/2026).
27 Haynes, S. E. *et al.* The P2Y12 receptor regulates microglial activation by extracellular nucleotides. *Nature Neuroscience 2006 9:12* **9** (2006-11-19).
28 Goldmann, T. *et al.* Origin, fate and dynamics of macrophages at central nervous system interfaces. *Nature Immunology 2016 17:7* **17** (2016-05-02).
29 Butovsky, O. *et al.* Identification of a unique TGF-β–dependent molecular and functional signature in microglia. *Nature Neuroscience 2013 17:1* **17** (2013-12-08).
30 Shemer, A. *et al.* Engrafted parenchymal brain macrophages differ from microglia in transcriptome, chromatin landscape and response to challenge. *Nature Communications 2018 9:1* **9** (2018-12-06).
31 Bennett, F. C. *et al.* A Combination of Ontogeny and CNS Environment Establishes Microglial Identity. *Neuron* **98** (2018/06/27).
32 Fuster, J. J. *et al.* Clonal hematopoiesis associated with TET2 deficiency accelerates atherosclerosis development in mice. *Science* **355** (2017-02-24).
33 Buttgereit, A. *et al.* Sall1 is a transcriptional regulator defining microglia identity and function. *Nature Immunology 2016 17:12* **17** (2016-10-24).
34 Zhou, Y. *et al.* Human and mouse single-nucleus transcriptomics reveal TREM2-dependent and TREM2-independent cellular responses in Alzheimer's disease. *Nature Medicine 2020 26:1* **26** (2020-01-13).